NUMERICAL INVESTIGATION ON EFFECTS OF PRIMER CONFIGURATION IN PROPELLANT CHAMBER OF GUN SYSTEM

Hiroaki Miura[1], Akiko Matsuo[1], Yuichi Nakamura[2] and Toshio Ishida[2]

[1]Keio University, 3-14-1 Hiyoshi, Kohoku-ku, Yokohama, 223-8522 Japan
[2]NOF Corporation, 61-1 Kitakomatsudai, Taketoyo-cho, Chita-gun, AICHI, 470-2398 Japan

Effects of primer configuration in the combustion chamber of a large calibre gun system utilizing solid propellant of smokeless gunpowder on the ignition performance such as the formation of differential pressure between the breech pressure and the projectile base pressure are numerically investigated. The mechanisms of generating the negative differential pressure are especially examined with various lengths of primer. The solid/gas two-phase fluid dynamics code for two-dimensional axisymmetric calculation of Eulerian gas flow and discrete solid propellant particles simulates the movement of solid propellant grains and the formation of pressure gradients in the chamber in the ignition process. The pressure histories at the inner wall of the chamber are compared with the experimental data for validation. It is shown by the simulations that larger differential pressure occurs at the initial combustion of the propellant in the case of shorter primer.

INTRODUCTION

The aim of promoting design of gun system is to make the projectile velocity at the muzzle higher and the internal pressure lower, as possible. Additionally, the igniting operation for solid propellant should be performed well, considering the differential pressure between the breech and the projectile base. Because of the modern transformation of the projectile base from flat form to complicated form and the extension of the base tail length, the length of primer that contains the igniter in the propellant chamber tends to be shortened. The effects of this shortening on the interior ballistics events need to be predicted in the design stage. The relation between this shortening and the negative differential pressure, in which the projectile base pressure is higher than the breech pressure, is of important concern. The appearance of the negative differential pressure indicates that undesirable pressure waves propagate in the propellant chamber. In order to protect the chamber wall and the projectile base from destructive pressure wave, the developmental mechanism of negative differential

pressure should be found out and the igniter system must be designed not to form the strong negative differential pressure in the firing process.

In this study, the interior ballistics simulations in the propellant chamber with various lengths of the primer are carried out using the two-dimensional axisymmetric two-phase fluid dynamics code. The simulated results are compared with the experimental data for validation, and the effect of the primer length on the chamber pressure is discussed.

DESCRIPTION OF CODE

Gas phase and solid phase flows are assumed to coexist in the propellant chamber. The gas phase is composed of propellant combustion gas, igniter combustion gas and air. The solid phase is composed of solid propellant. In the computational domain, the given macroscopic volume is divided into the volume of gas and solid, and the volume fraction for each phase is used in the Eulerian governing equations. Porosity α represents the fraction of a unit macroscopic volume occupied by the gas phase, and $\alpha_{\mathrm{p}} = 1-\alpha$ is the volume fraction of the solid phase. The gas phase is considered as compressible inviscid flow, and its governing equations contain the term of mass and energy generation by the solid decomposition. The balance equations for mass, momentum, energy and masses of components are given by,

$$\frac{\partial}{\partial t}(\alpha\rho) + \nabla\cdot(\alpha\rho\mathbf{u}) = \dot{m} + \dot{m}_{ig} \tag{1}$$

$$\frac{\partial}{\partial t}(\alpha\rho\mathbf{u}) + \nabla\cdot(\alpha\rho\mathbf{u}\mathbf{u}) = -\alpha\nabla p - \mathbf{f}_s + \dot{m}\mathbf{u}_p \tag{2}$$

$$\frac{\partial}{\partial t}(\alpha e) + \nabla\cdot\{\alpha(e+p)\mathbf{u}\} = -\mathbf{f}_s\cdot\mathbf{u}_p + \dot{m}\left(q_e + \frac{\mathbf{u}_p\cdot\mathbf{u}_p}{2}\right) + \dot{m}_{ig}q_{ig} - q_p \tag{3}$$

$$\frac{\partial}{\partial t}(\alpha\rho Y_{pr}) + \nabla\cdot(\alpha\rho Y_{pr}\mathbf{u}) = \dot{m},\ \frac{\partial}{\partial t}(\alpha\rho Y_{ig}) + \nabla\cdot(\alpha\rho Y_{ig}\mathbf{u}) = \dot{m}_{ig},\ \frac{\partial}{\partial t}(\alpha\rho Y_a) + \nabla\cdot(\alpha\rho Y_a\mathbf{u}) = 0 \tag{4}$$

where ρ is the gas density, $\mathbf{u}$ is the gas phase velocity vector, p is the pressure and e is the total energy. The relation between the mass fractions of three components in gas phase is given by $Y_{pr} + Y_{ig} + Y_a = 1$ in which subscript pr stands for the propellant combustion gas, subscript ig stands for the igniter combustion gas and subscript a stands for the air. The right hand side in Eq. (1) contains the rate of mass decomposition $\dot{m}$. The vector $\mathbf{f}_s$ represents the interphase drag and $\mathbf{u}_p$ is the solid phase velocity vector in which subscript p stands for the propellant. The right hand side in Eq. (3) contains the combustion heat q_e and q_{ig}, and the heat transfer term q_p.

The solid phase is considered as incompressible flow, and in its governing equation the solid propellants are regarded to have constant density. In the simulations, the distribution of solid propellant grain is represented by the volume fraction of solid phase α_p, which is determined from the distribution of representative particles. These particles have the information of the extent of burning progress, the volume and temperature of solid grains, and solid phase velocity. The field interphase properties are also determined by mapping the interphase data of the representative particles, considering the assigned volume of each particle varying with time according to the extent of burning progress. The balance equation of the solid phase for momentum is given by,

$$\frac{\partial}{\partial t}\left(\alpha_p \rho_p \mathbf{u}_p\right)+\nabla\cdot\left(\alpha_p \rho_p \mathbf{u}_p \mathbf{u}_p\right)=-\alpha_p \nabla p-\mathbf{f}_i+\mathbf{f}_s-\dot{m}\mathbf{u}_p \tag{5}$$

where ρ_p is the solid propellant density and $\mathbf{f}_i$ represents the intergranular force.

The gas satisfies the covolume equation of state,

$$p=\frac{RT}{\left(1/\rho-b\right)}, \qquad \varepsilon=C_v T \tag{6}$$

where p is the pressure, T is the temperature, ρ is the gas density, R is the gas constant, ε is the internal energy of gas and C_v is the specific heat at constant volume.

The volume of the solid phase decreases by propellant combustion. The rate of mass decomposition and the linear burning rate on each grain surfaces are respectively given by,

$$\dot{m}=\left(1-\alpha\right)\rho_p \frac{S_p}{V_p} r, \qquad r=a\cdot p^n \tag{7}$$

where S_p is the particle surface, V_p is the particle volume and p is the ambient pressure. a and n are empirical coefficients. The interphase drag in the chamber is given in the following form [1],

$$f_s=\frac{1-\alpha}{D_{pe}}\rho\left(u-u_p\right)\left|u-u_p\right| f_{sc} \tag{8}$$

$$f_{sc}=\begin{Bmatrix} \dfrac{2.5\lambda^{2.17}}{\mathrm{Re}_p^{\,0.081}}C & \left(\alpha_e \le \alpha_{e0}\right) \\ \max\left[\dfrac{2.5\lambda^{2.17}}{\mathrm{Re}_p^{\,0.081}}C\left(\dfrac{1-\alpha_e}{1-\alpha_{e0}}\dfrac{\alpha_{e0}}{\alpha_e}\right)^{0.45},\ f_{min}\right] & \left(\alpha_{e0}<\alpha_e \le 1\right) \end{Bmatrix},$$

$$\lambda = \frac{0.5 + L_P / D_P}{\left(3L_P / 2D_P\right)^{2/3}}, \quad \mathrm{Re}_p = \frac{\rho |u - u_P| D_{pe}}{\mu}$$

where L_p is the length of a cylindrical grain and D_p is its diameter. The coefficients are decided as $C = 0.85\chi$, $\chi = 20$ and $f_{min} = 0.75$. The interphase heat transfer [1] is given by the following equations,

$$q_p = n_p S_p q = (1-\alpha)\frac{S_p}{V_p} q \tag{9}$$

$$q = h(T_g - T_p) \tag{10}$$

$$Nu_p \equiv \frac{hD_p}{k_f} = 0.4\,\mathrm{Pr}^{1/3}\,\mathrm{Re}_p^{2/3}, \quad \mathrm{Pr} \equiv \frac{C_p \mu}{k} = \frac{4\gamma}{9\gamma - 5} \tag{11}$$

where h is the thermal transfer coefficient, T_g is the temperature of gas phase and T_p is the temperature of a solid particle. Energy of solid particle obtained by heat transfer, which contributes to the increase of solid particle temperature, is expressed by,

$$H = \int S_p q dt = m_p c\left(T_p - T_{p0}\right) \tag{12}$$

where m_p is a solid particle mass, c is specific heat of solid particle and T_{p0} is the initial temperature of a solid particle. The ignition of the solid propellant grain is assumed to occur when the ambient gas temperature T_g exceeds a pre-determined value. The intergranular force $\mathbf{f}_i$ is given by next formula [2].

$$\mathbf{f}_i = \nabla\sigma, \quad \sigma = \rho a_1^2 \alpha_0^2 \left(\frac{1}{\alpha} - \frac{1}{\alpha_0}\right) \tag{13}$$

The discretization method of convection term is the simple high-resolution upwind scheme (SHUS) [3]. Third-order space accuracy is obtained using monotonic upwind scheme for conservation laws for the primitive variable interpolation. The time integral method is the 2-step Runge-Kutta method.

NUMERICAL TARGETS

In this study, the simulation results are compared with the experimental data for validation. The experiments were performed using a combustion vessel with a rupture disk, shown in Figure 1. The inner diameter of the vessel is 148 mm and the internal

length is 550 mm. The conditions of the vessel configuration are listed in Table 1, and the characteristics of charged triple-base solid propellant are listed in Table 2. The pressures in the propellant chamber were measured by the piezoelectric gauges. The three gauges were installed near the breech (P1), near the rupture disk (P3) and in the middle of those two gauges (P2). An optical fiber cable was installed near the rupture disk to measure a shearing time of the rupture disk. The cases for the primer length L_{ig}=300, 200 and 100 mm were performed. In the primer, straight Benite strands were charged as the igniter. The primers have 28 holes of ϕ5 for L_{ig}=300 mm, 18 holes of ϕ5 for L_{ig}=200 mm and 8 holes of ϕ5 for L_{ig}=100 mm.

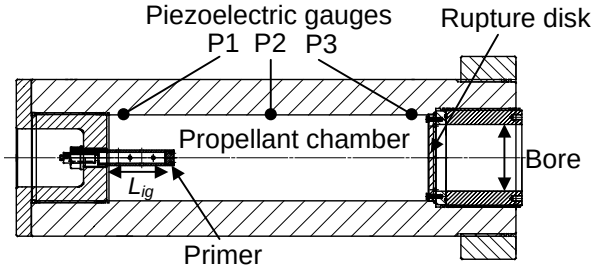

Figure 1. Combustion vessel with the rupture disk

Table 1. Conditions of the experiment

Term	Data
Chamber diameter (mm)	148
Bore diameter (mm)	115
Length between breech and rupture disk (mm)	550
Propellant mass (kg)	8.4
Propellant geometry	Hexagonal 19-perforated
Size of propellant grain, perforation diameter (mm)	ϕ15x15, 0.5
Igniter mass (g)	65 (L_{ig}=300 mm) 43 (L_{ig}=200 mm) 22 (L_{ig}=100 mm)

Table 2. Characteristics of solid propellant

Term	Data
Impetus (J/g)	1026
Specific heat ratio	1.245
Density (kg/m^3)	1680
Covolume (cm^3/kg)	1062
Propellant thermal conductivity* (W/m/K)	0.2218
Propellant thermal diffusivity* (mm^2/s)	0.08677
Ignition temperature* (K)	444

* : The data are from the AGARD Gun condition [4]

Figure 2 shows the computational domain and representative particles in L_{ig}=300 mm case, where the number of the base grid points is 433x38, that of the overlapping grid points on the rupture disk is 24x38 and that of the representative particles is 616. In all of the cases, the pressure data shown in Figure 3 is applied in the primer with time, and the temperature in the primer is fixed at the igniter adiabatic flame temperature 1981 K. The mass of rupture disk is set to 1.23 kg in the simulation. From the experimental measurement, the pressures of P3 at the shearing time are set to 150 MPa for L_{ig}=300 mm, 160 MPa for L_{ig}=200 mm and 150 MPa for L_{ig}=100 mm. The total area

of the primer slits in the two-dimensional axisymmetric simulation is adjusted to be equal to the total area of the primer holes in the experiments. For the initial condition in the chamber, the temperature is uniformly 293 K and the pressure is uniformly 101 kPa.

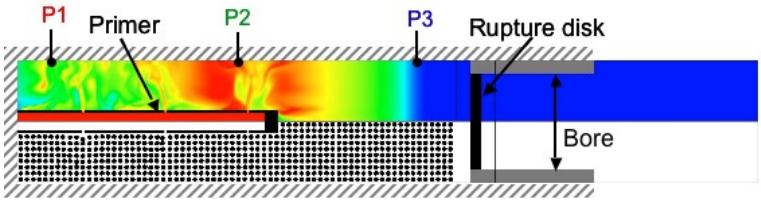

Figure 2. Computational domain of the propellant chamber for the case of L_{ig}=300 mm

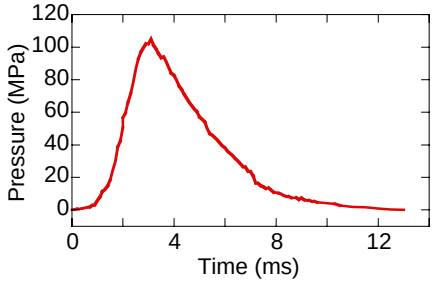

Figure 3. Experimental pressure history in the primer of L_{ig}=100 mm

RESULTS AND DISCUSSIONS

Figure 4 shows the simulated time histories of P1 and P3, and the differential pressure P1-P3 with the experimental results for the cases of (a) L_{ig}=300 mm, (b) L_{ig}=200 mm and (c) L_{ig}=100 mm. In the experiment, P1 increases at first because of the igniter gas flows exhausted from the primer near the breech, and subsequently P3 rises and exceeds P1 in all of the cases. As the primer is shortened, the pressure rise at P3 is delayed. After that, P1 becomes larger than P3. It should be noted that the history of P1 has an inflection point in each case right after the differential pressure reaches the minimum value. In the experiment, P1 and P3 rise rapidly in the latter stage and the maximum pressure of P1 gets larger as the primer is shortened. Furthermore, the minimum value of the differential pressure between P1 and P3 becomes lower with the shortening of the primer. In the simulation, the experimental tendency for the rate of pressure rise and the maximum pressure to become larger with the shortening of primer is reproduced. Additionally, the appearance of negative differential pressure and inflection point in the history of P1 are reproduced in each case, although the simulated negative differential pressure is weaker than the experiment in the case of L_{ig}=100 mm.

The simulated results reveal the events in the propellant chamber through the ignition process. Figure 5 shows (a) the pressure distribution and (b) the porosity distribution in the axial direction in the propellant chamber at each time using bulk

average in the radial direction for L_{ig}=300 mm, and similarly (c) the pressure distribution and (d) the porosity distribution for L_{ig}=200 mm. As shown in the pressure distributions at t=1.5 ms and t=2.5 ms, the breech pressure rises earlier than the pressure at rupture disk in both the cases since the primer is located near the breech. By comparing the porosity distributions at t=1.5 ms and t=2.5 ms, the concentrated part of solid phase volume (small porosity parts) is observed to be formed near the rupture disk because of the movement of solid propellant caused by the pressure gradients. At t=3.5 ms, however, the pressure at the rupture disk becomes larger than the breech pressure in

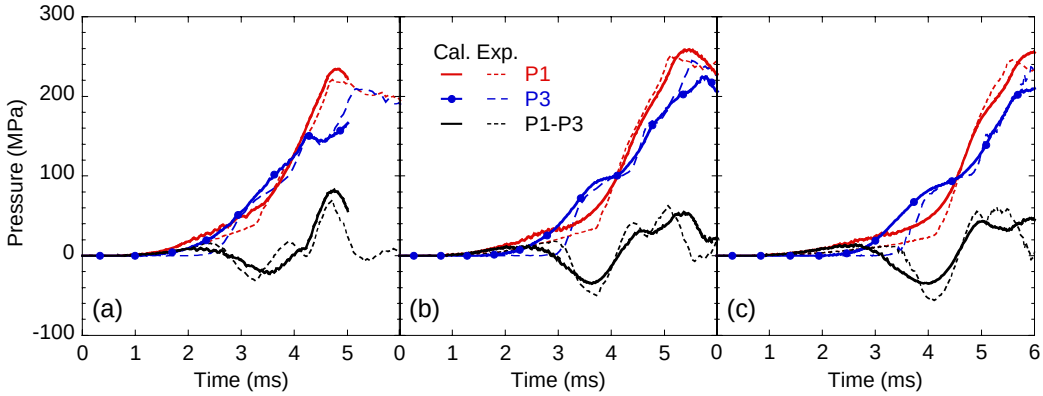

Figure 4. Time histories of P1, P3 and P1-P3 for the cases of (a) L_{ig}=300, (b) 200 and (c) 100 mm

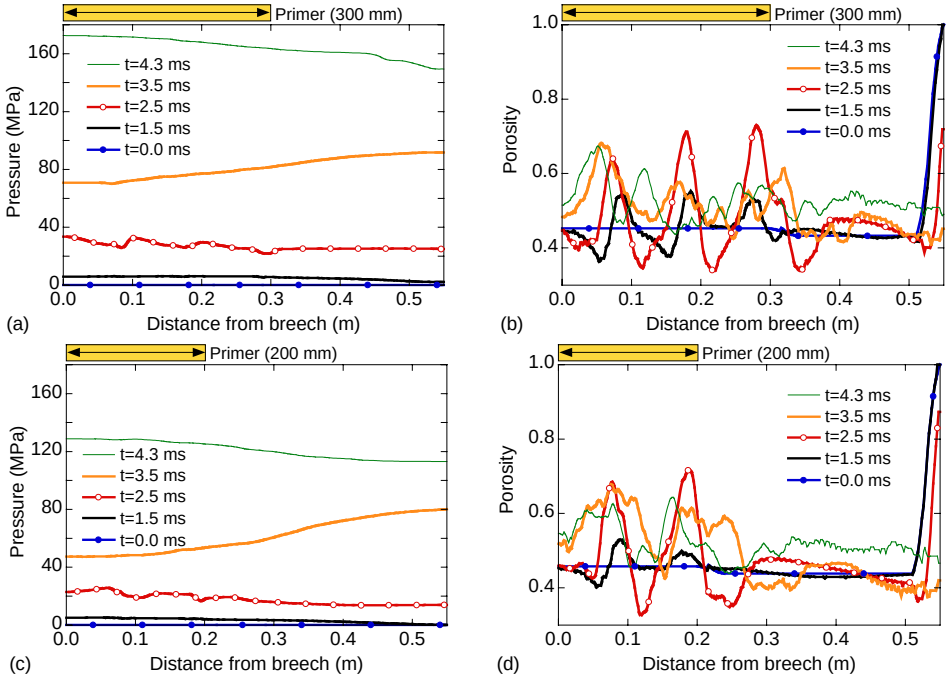

Figure 5. Pressure distribution and porosity distribution in the axial direction in the chamber at each time for the cases of L_{ig}=300 and 200 mm

both cases. By this time, the concentrated part of solid phase volume has reached the rupture disk, and the porosity in the vicinity of the primer has increased. These movements of the solid grains cause the enhancement of the propellant combustion at the rupture disk and the decompression near the primer. This is the reason why P3 exceeds P1 in the early stage of each case. The early rapid rise of P3 tends to increase with the shortening of the primer in the experiment, which is caused by the increase of the axial movement of solid grains as the primer length is shortened. By t=4.3 ms, the high pressure part at the rupture disk has moved to the breech. The pressure increase by the propellant combustion near the breech is enhanced and consequently P1 again exceeds P3. This process explains why the history of P1 has an inflection point right after the minimum differential pressure in each case. The above results reveal that the differential pressure is caused by the movement of solid grains in the chamber, depending on the primer length.

CONCLUSION

The interior ballistics simulations in a propellant chamber with different lengths of primer near the breech were carried out, using solid/gas two-phase fluid dynamics code of two-dimensional axisymmetric calculation method. The negative differential pressures between the breech and the rupture disk (on the projectile base) measured in the experiment were well predicted by the simulations excluding the shortest primer case. In the process of igniting the solid propellant, the propellant grains were accelerated toward the rupture disk by the igniter gas flows from the primer and pressure gradients. From the simulated results, it was concluded that this movement of solid grains caused the stronger negative differential pressure for the shortened primer in the experiment.

REFERENCES

[1] M.J. Nusca, P.J. Conroy, “Multiphase CFD Simulations of Solid Propellant Combustion in Gun systems,” *Department of Defense High Performance Computing Modernization Program users group conference*, 2001.
[2] P.J. Conroy, D.E. Kooker, “Implications of Gun Propellant Bed Rheology,” *ARL-TR-80, U.S. Army Research Laboratory*, 1993.
[3] E. Shima, T. Jounouchi, “Role of Computational Fluid Dynamics in Aeronautical Engineering (No.12), Formulation and Verification of Uni-Particle Upwind Schemes for the Euler Equations,” *Proceedings of the 12th NAL Symposium on Aircraft Computational Aerodynamics*, Japan, 1995, pp.255-260.
[4] “Fluid Dynamics Aspects of Internal Ballistics,” *AGARD Advisory Report No.172*, 1982.